energies

MDPI

Review

Performance Improvement for Building Integrated Photovoltaics in Practice: A Review

Yiqing Dai * and Yu Bai

Department of Civil Engineering, Monash University, Clayton, VIC 3800, Australia; yu.bai@monash.edu
* Correspondence: yiqing.dai@monash.edu

Abstract: Building integrated photovoltaic (BIPV) technologies are promising and practical for sustainable energy harvesting in buildings. BIPV products are commercially available, but their electrical power outputs in practice are negatively affected by several factors in outdoor environments. Performance improvement of BIPV applications requires mitigation approaches based on an understanding of these factors. A review was, therefore, conducted on this issue in order to providing guidance for practical applications in terms of the selection of proper PV technologies, temperature management, solar irradiation enhancement and avoidance of excessive mechanical strain. First, major types of PV cells used in BIPV applications were comparatively studied in terms of their electrical performances in laboratorial and outdoor environments. Second, temperature elevations were widely reported in outdoor BIPV applications, which may cause efficiency degradation, and the mitigation approaches may include air-flow ventilation, water circulation and utilization of phase change materials. The heat collected from the PV cells may also be further utilized. Third, mechanical strains may be transferred to the integrated PV cells in BIPV applications, and their effects on electrical performance PV cells were also discussed. In addition, the power output of BIPV systems increases with the solar irradiation received by the PV cells, which may be improved in terms of the location, azimuth and tilt of the cells and the transmittance of surface glazing. Suggestions for practical applications and further research opportunities were, therefore, provided.

Keywords: building integrated photovoltaics (BIPV); solar cell; electrical response; mechanical loading; sustainability; energy harvesting

Citation: Dai, Y.; Bai, Y. Performance Improvement for Building Integrated Photovoltaics in Practice: A Review. *Energies* **2021**, *14*, 178. https://doi.org/10.3390/en14010178

Received: 28 November 2020
Accepted: 27 December 2020
Published: 31 December 2020

1. Introduction

Photovoltaic (PV) panels mounted on rooftops are able to generate electricity from solar energy without emitting greenhouse gases in operation or taking up additional ground. This has been well practiced [1] and also been widely supported by Feed-in Tariff programs (e.g., in Europe [2], North America [3], Asia [4] and Australia [5]). In order to eliminate the structural mounting cost and enhance the aesthetic appearance of the roof-mounted PV panels, an optimized prototype was fabricated by integrating the PV cells into roof tiles in 1994, and it was reported that the total cost for the PV system was reduced by 14 to 26% [6]. Such building elements with integrated PV cells are referred to as building integrated photovoltaics (BIPV) in literature [7,8]. BIPV applications in the early stage before 1996 were well reviewed in [9], where ten categories of BIPV applications were introduced including rooftop applications, facades, windows, skylights and shading systems. PV cells used in these applications were mainly based on polycrystalline and amorphous silicon [9]. Recent BIPV practices have also been extensively reviewed [10], where a wide range of commercial BIPV products and practical BIPV applications were presented, and some innovations may include applications in new scenarios such as noise barriers [11] and optimizations in energy storage systems [12]. In terms of the market share, BIPV in facades and roofs plays the dominant role, and according to a review on the market share in the BIPV field in 2017, roof applications account for a market share of

about 80% and facade applications account for about 20%, while the market share of other BIPV applications is minor [10].

Policies for encouraging BIPV applications have been initiated in recent decades, among which the zero-energy or net-zero energy building is a major concept [13,14]. Zero-energy buildings are required to produce equivalent energy (e.g., from renewable technologies) to balance their energy consumption [14,15]. For example, it was reported that, all new public buildings in Japan should be zero energy by 2020 [16]. BIPV applications are usually suggested as the core solution for achieving zero-energy buildings. However, Feed-in Tariff (FiT) programs for renewable energies have provided monetary incentives to BIPV applications, and their effects on promotion of BIPV are direct and obvious. For example, the rate of FiT in Southeast Queensland, Australia, is presented in Figure 1 with the annual number of installed small-scale household PV systems (mainly roof-mounted panels) [17]. It can be seen in Figure 1 that from 2008 to 2012, a relatively high FiT rate of AUD 44 c/kWh was provided and the annual installed number of small-scale PV panel systems increased rapidly from about 42,000 in 2008 to about 1,674,000 in 2012, while the installed number dropped to, for example, 443,000 in 2016 when the FiT rate was reduced to less than AUD 10 c/kWh. National FiT programs were initiated in China from 2011 with a rate of 1.15 CNY/kWh, and this was reduced to 0.9–1.0 CNY/kWh in 2013 and 0.80–0.98 CNY/kWh in 2015 [18]. In similar programs in Germany, the FiT rate was 0.51 EUR/kWh in 2000 and adapted to about 0.55 EUR/kWh in 2003, about 0.25 EUR/kWh in 2009 and about 0.12 EUR/kWh in 2012 [19]. It may be noticed that the expansion of BIPV applications to some extent relies on FiT programs. However, the global trend in reduction in the FiT rate made the BIPV market unable to reach the prospects made in some early research. For example, the worldwide BIPV market was estimated to grow at 40% annually from USD 1.1 billion in 2017 to over USD 2.7 billion in 2021 [20], and the installed capacity of BIPV was predicted in 2014 to have an annual growth rate of 18.7% to reach a total installed capacity of 5.4 GW by 2019 worldwide [21].

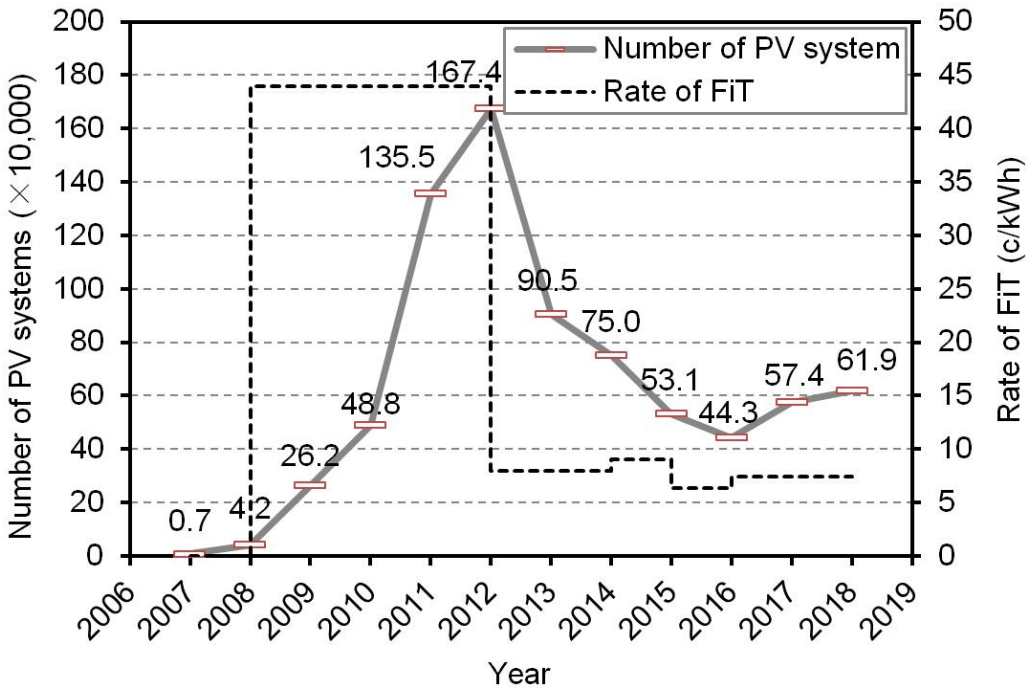

Figure 1. Rate of FiT and annual number of installed small-scale PV panel systems from 2007 to 2018 in Southeast Queensland, Australia (adapted from [17]).

In order to maintain the cost effectiveness of BIPV applications at the background of the global reduction in the FiT rate for PV applications, the overall power output

of the integrated PV cells is expected to be enhanced and, therefore, enhances the cost effectiveness. As shown in Figure 2, the power output is determined by the actual efficiency and the received solar irradiation of the integrated PV cells, and therefore, the related influencing parameters are investigated in this work.

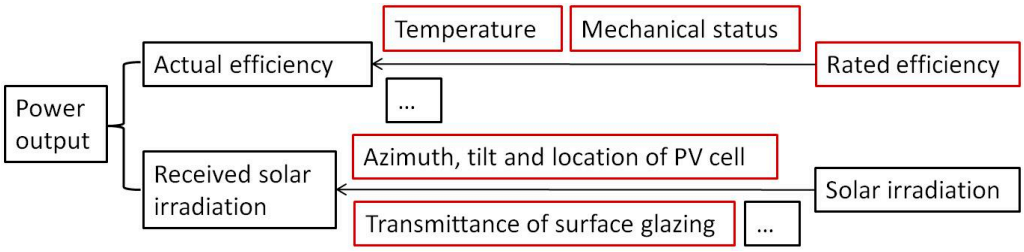

Figure 2. Schematic of approaches to improve power output.

The rated efficiency is a core parameter to quantify the ability of PV cells to transfer solar energy into electricity, and this is defined as the ratio between the generated electricity and the received solar energy at the standard test conditions (i.e., 1000 W/m^2 solar intensity and a temperature of 25 °C [21,22]). A wide range of research has been conducted to enhance the rated efficiency of PV cells, and the highest confirmed efficiencies for a range of PV cell technologies are summarized in "solar cell efficiency tables [23]", with updates every six months since 1993. For example, the present efficiency records for the aforementioned polycrystalline silicon PV and amorphous silicon (a-Si) PV cells usually used in BIPV are 26.7 and 10.2%, respectively [23]. However, it is usually time-consuming and laborious to develop an innovative PV cell with enhanced efficiency and durability, and such innovative PV cells are usually not affordable for building applications. For BIPV applications, it is more practical to compare the existing types of PV cells and then select the proper one for practice.

The efficiency of PV cells may be negatively affected by several factors in outdoor environments such as temperature and mechanical status of the PV cells as shown in Figure 2, and the actual cell efficiency is usually smaller than the rated efficiency. For example, the actual efficiency is only about 6% for PV panels with a rated efficiency of 11.9% according to annual monitoring of roof-mounted PV panels in Bangalore, India [24]. Mitigation approaches may, therefore, be proposed from the aspects of these factors.

First, the efficiencies of PV cells usually present a decreasing trend for temperatures over 25 °C [25,26]. Elevated temperatures have been widely reported in operating PV cells since only a part (usually smaller than 30%) of the absorbed solar energy is transferred into electricity, while the others become heat [26,27]. In existing research, temperature mitigation for operating PV cells is realized by taking away the excessive heat through certain media. Air flow (through ventilation), water and phase change materials have been used in this regard; the three types of approaches have been widely investigated, and their effectiveness in temperature mitigation and cell efficiency enhancement have been reviewed in literature [28,29]. However, in practical applications, the heat collected from the PV cells may be further utilized [30,31]. Therefore, in order to properly evaluate the actual energy-harvesting performance and cost effectiveness of BIPV systems with temperature mitigation approaches, the electricity generated and the heat collected for utilization should both be considered. It appears that literature reviews in this regard are very limited.

Second, mechanical status also affects the power output of BIPV applications [32,33], and integrated PV cells may be subjected to certain mechanical strain, although they are supposed to be applied in scenarios without structural loads. Studies have been conducted to understand the strain effects on the electrical performance of the PV cells, but systematic review is required to understand the applicable mechanical scenarios for different types of PV cells. It should be aware that BIPV applications are currently excluded from load-

carrying scenarios, which take up the major exterior surfaces of buildings, while such research may break such limitation.

In addition, as shown in Figure 2, the total solar energy received by the PV cells is determined by the sunlight intensity and the position and configuration of the PV cells [34,35]. Unlike the constant light intensity provided in laboratorial conditions, the sunlight received by the PV cells in outdoor environments varies with a wide range of factors such as location, azimuth, tilt, time and weather conditions. In conventional BIPV applications, the azimuth and tilt of integrated PV cells are determined by the facades or roofs, while in several recent studies, PV cells were associated with a different tilt or azimuth with the building envelope [36]. Future literature reviews in this regard are needed to understand the effectiveness of these approaches.

The main objective of this review is to present the approaches, in use or recently proposed, to enhance the power output of BIPV applications from the aspects of optimizing their operational conditions in outdoor environments. Such optimization requires understanding of electrical properties of PV cells used in BIPV applications, which are, therefore, firstly reviewed. Second, approaches for temperature mitigation using air flow ventilation, water circulation and phase change materials were presented, and their capacities to harvest solar energy were evaluated considering both the electricity generated and the heat collected for utilization. Third, effects of mechanical strain on the electrical performance of integrated PV cells were reviewed in order to investigate applicable load-carrying scenarios of different BIPV configurations, and the work in this regard is still very limited at present. In addition, in several recent studies, PV cells were associated with a different tilt or azimuth with the facades or roofs, providing new solutions to enhance the solar irradiation received by the PV cells. Therefore, approaches to enhance the solar irradiation were reviewed to include this recent research. Suggestions for optimization of BIPV applications in practice were also provided.

2. Performance of Different Types of PV Cells

2.1. Main Parameters for Consideration

In order to understand the main parameters associated with the electrical power output of PV cells in BIPV applications, the formula in calculating the power output is provided as Equation (1). Theoretically, the amount of electricity generated, $P(t)$, by an integrated PV cell is determined by the actual efficiency and projected area of the PV cells, the received solar intensity and the operation duration according to the following equation [37],

$$P(t) = \int_0^t E(t)I(t)A(t)dt \quad (1)$$

where $E(t)$ is the actual efficiency of the PV cell at time t; $I(t)$ is the solar intensity at time t; and $A(t)$ is the projected area of the PV cell at time t.

The actual efficiency of a PV cell is related to the rated efficiency and the effects from the environment. Considering the cost, toxicity and commercialization, PV cells based on crystalline silicon (c-Si), amorphous silicon (a-Si), copper indium gallium selenide (CIGS) and cadmium telluride (CdTe) materials have been used in practical BIPV applications [38,39] and their up-to-date cell efficiencies are listed in Table 1 according to [23] together with their market share in 2018 Q4 and 2019 Q1 [40]. Since the cell efficiency was tested based on small samples with a typical area of 1 cm^2 while the actual efficiency is affected by cell dimensions, encapsulation and other procedures in commercialization, the efficiencies for PV modules and commercial PV panels are also provided in Table 1 [23,41]. Furthermore, the efficiencies listed in Table 1 are obtained in the standard test conditions, i.e., solar intensity of 1000 W/m^2 and a cell temperature of 25 °C [21,22]. It can be seen in Table 1 that the c-Si technologies are usually associated with the highest efficiency, and the a-Si technologies have the lowest.

Table 1. Main properties of different types of PV cells.

PV Technologies	c-Si	a-Si	CIGS	CdTe	Organic
Cell efficiency (%) [23]	26.7 ± 0.5	10.2 ± 0.3 *	23.35 ± 0.5	21.0 ± 0.4	13.45 ± 0.2
Area of the cell (cm^2) [23]	79.0	1.0	1.0	1.0	1.0
Module efficiency (%) [23]	24.4 ± 0.5	12.3 ± 0.3	19.2 ± 0.5	19.0 ± 0.9	8.7 ± 0.3
Area of the module (cm^2) [23]	13,177	14,322	841	23,573	802
Temperature coefficient (%) [42]	−0.37 to −0.52	−0.10 to −0.30	−0.33 to −0.50	−0.18 to −0.36	/
Efficiency of commercial panel (%) [41]	14.9 to 19.0	9.5	12.7 to 16.0	8.5 to 14.0	/
Energy payback time (year) ** [43]	2.9 to 3.3	3.1	2.9	2.5	/
Market share (%) [40]	95.70	0.05	1.13	3.12	/

* After 1000 h exposure to solar irradiance of 1000 W/m^2. ** Estimated at the condition of 1117 kWh/m^2 annual solar irradiation and 0.75 performance ratio.

Dye-sensitive and Perovskite PV cells have also been employed in the development of BIPV components. For example, dye-sensitive PV cells were encapsulated in translucent glass fiber reinforced polymer (GFRP) laminates for BIPV applications [44], and they were also experimentally investigated for window applications [45]. Perovskite PV cells were subjected to tensile loading to evaluate the feasibility for BIPV applications in load-carrying scenarios [32]. However, BIPV applications in large scale practices with these PV technologies are still limited, and their information is, therefore, not included in Table 1.

Energy payback time is also used to quantify the cost or energy effectiveness. It is defined as the number of years needed for the PV cells to produce enough electricity to cover the energy consumed in production [46]. However, the estimations of payback time are inconsistent among different research [39,43] since the power output of a PV system largely depends on the applied environment. The energy payback time for several PV types based on results from the same estimation method is listed in Table 1 [43], providing a reference for the energy effectiveness of the PV cells. For example, an energy payback time of 3.1 years for a-Si cells means the electricity generated in 3.1 years could pay back the energy in producing the cells. However, the payback time for BIPV applications may be much longer due to more materials, time and labor required for manufacturing. For example, the energy payback time for a rooftop BIPV system with c-Si PV cells in Hong Kong was estimated to be 7 to 20 years depending on orientations and tilts of the panels [27].

Temperature coefficients are used to quantify the dependence of power output of PV cells on elevated temperatures. Existing results have shown that the power output of the PV cells may decrease approximately in linearity with temperatures over 25 °C [25,42], and the decrease ratio is referred to as the temperature coefficient. For example, as shown in Table 1, the temperature coefficient for c-Si PV cells is −0.37 to −0.52%. This means when the temperature is over 25 °C, the power output of c-Si PV cells may decrease by 0.37 to 0.52% for a temperature rise of 1 °C.

2.2. Comparison of Different Types of PV Cells

It can be seen from Table 1 that the c-Si technologies achieve the highest efficiency in terms of cell, module and commercial panels and are the dominant PV types with a market share of 95.7%. However, since glass encapsulation and a frame are used to protect brittle c-Si PV cells, a typical thickness of traditional c-Si PV panels is several centimeters, which is much thicker than thin-film PV cells. For example, the thin film a-Si PV cells have a total thickness of only about 1 mm and the organic PV cells have a thickness of less than 0.1 mm [33]. Thin-film c-Si PV cells have been developed in a laboratory and are not commercially available [47]. The thickness and brittleness of c-Si PV panels made them difficult for integration with building materials; therefore, they are usually mounted by additional frames on roofs [27,48] or as facades [49]. Such PV panels mounted by frames without integration into building components are also considered as BIPV in this research, although they may be referred to as building-applied photovoltaics (BAPV) in literature [8].

As shown in Table 1, the a-Si PV cells are associated with a relatively low efficiency. The progress to enhance their efficiency seems relatively slow considering that the efficiency of a-Si PV cells reached 13.0% in 1997 [50]. However, thin-film flexible a-Si PV cells have been commercially available for at least two decades, and they have shown potential for the development of BIPV integrations also with a relatively smaller degradation at elevated temperatures as shown in Table 1.

CIGS PV and CdTe PV cells have moderate efficiencies comparing to c-Si or a-Si PV cells. CdTe PV cells have the shortest energy payback time, indicating a high energy effectiveness. Their BIPV applications include roofs and facades [51]. Flexible PV cells based on CdTe technology have also been developed [52], and BIPV windows have been manufactured based on semitransparent CdTe PV cells [53], showing their superior potentials. However, a concern has been raised for their application in residential buildings considering the cadmium element in cadmium telluride as a core material in the PV cells is toxic especially in fire [54]. Most CIGS PV cells also contain cadmium, and this may hinder their wide applications in buildings. Therefore, CIGS PV cells have been developed without cadmium [23].

Although organic PV cells have a rated efficiency of 13.45% (see Table 1), the efficiencies of commercial organic PV cell tapes are as low as 2–6% [33]. Large scale applications of organic PV cells are limited by their high producing cost, low efficiency and short service life [55]. Three types of semitransparent dye-sensitive PV cells with different colors and efficiencies were produced for glazing system with the efficiencies of 2.51, 4.49 and 5.93%, respectively [45]. Dye-sensitive PV cells have also been encapsulated into GFRP plates to develop BIPV components where their resistance to temperature cycles was investigated [44]. The perovskite material is an emerging technology, and they have been made into thin-film or flexible PV cells, transparent or with different colors, while most of them are currently not commercially available [56]. Effects of tensile strain on thin-film flexible Perovskite PV cells have been investigated for further BIPV applications, as reported in [32].

PV cells for large scale BIPV integrations have to be selected from commercially available products in consideration of their efficiency, payback time and temperature coefficient. In a short summary, the c-Si PV cells are associated with high efficiency but usually mounted on rooftops and facades. The a-Si PV cells have only a light market share but show potentials for large scale BIPV applications. The potential toxicity of CdTe PV and CIGS PV cells may hinder their applications in buildings.

3. Mitigation of Temperature Effects

As introduced, temperature mitigation for operating PV cells is realized by taking away the excessive heat by certain media in existing research. Air flow (through ventilation), water and phase change materials have been used in this regard, and the three types of approaches are correspondingly presented and individually discussed in this section.

3.1. Natural or Forced Ventilation

Temperature elevation is among the core factors causing power output reduction in PV cells in BIPV applications [25]. The most direct way to avoid excessive temperature elevation of the PV cells in operation is to maintain adequate ventilation. PV panels mounted by frames on rooftops and facades usually leave a gap between the building envelope as shown in Figure 3 [27,57]. Such a gap allows heat convection by air flow, and if the ventilation relies only on natural air flow, it is referred to as natural ventilation in literature [58]. For example, a roof-mounted PV panel is shown in Figure 3a, showing an air gap between the panels and the rooftop. According to estimations through computational fluid dynamics (CFD) simulation and experimental validation, a maximum reduction of 20 °C could be achieved by natural air flow in such gaps [59]. It should also be noted that air flow may be also powered by fans, and this ventilation method is then referred to as forced ventilation [60].

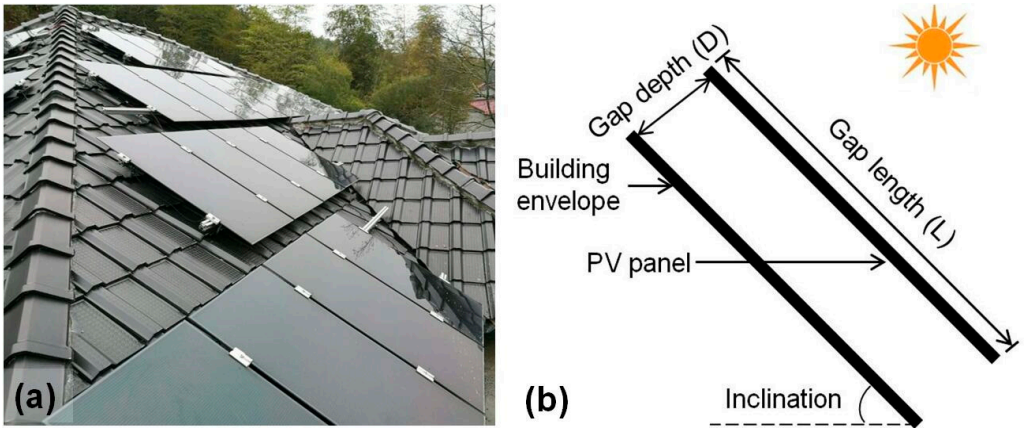

Figure 3. (**a**) CdTe PV panels mounted on the rooftop of a residential building in Zhejiang Province, China (courtesy of Zhiqian Liu) and (**b**) the analytical model for heat transferring between the PV panel and the building envelope.

The temperature difference between the operating PV cell and ambient environment is defined as ΔT, and proper dimensional parameters of the gap between the PV panel and building envelope have been investigated in several studies to mitigate the temperature elevation (i.e., ΔT). For example, two parallel fiber reinforced Bakelite plates, each with a dimension of about 2.0 m high and 0.8 m wide, were prepared as facade specimens in [61]. The surface of one plate was then covered by a series of thin metal heaters to simulate integrated PV cells. The specimens were placed vertically and associated with different gap depths and then subjected to different heating power levels to simulate temperature elevation of PV cells at different solar intensities. When the thermal status of the configurations became stable, temperatures at different locations of the surface with the heaters were measured. It was found that ΔT increased with the position of the measuring points until a height of 0.8 m. For the measuring points at higher positions, the temperature variation became minor. ΔT decreased when the gap depth increased from 3 to 5 or 10 cm, but remained unchanged when the depth increased from 10 to 16 cm. It was also found that if the heaters (as simulation of PV cells) were not continuously installed, ΔT could also be mitigated. In addition, it was shown that the heat flux levels applied in this study ranged from 75 to 200 W/m^2 [61].

In theoretical analyses and CFD simulations for the heat transfer behavior in BIPV facades and roofs with natural ventilation, the PV panels and wall were often simplified as two parallel plates with a surface heated from outside as shown in Figure 3b. The results showed that the length, depth and inclination of the gaps (see Figure 3b) would affect their temperature mitigation effects. When the inclination increases and the parallel plates change gradually from horizontal to vertical, the velocity of the air in the gap increases and, therefore, ΔT decreases. As a result, vertical BIPV facades are associated with a better ventilation condition than horizontal or pitched PV panels on rooftops [62]. The depth of the air gaps was found to have the most obvious effects on temperature mitigation [63]. Such mitigation effects of the air gaps increase with gap depth until the optimal value. The suggested gap depths reported in different research are summarized in Table 2, where the gap depth is referred to as D and its length is L as also shown in Figure 3b.

Table 2. Suggested gap depths for ventilation in building integrated photovoltaics (BIPV).

Suggested Gap Depth	Method	Ventilation Method	Scenario	Year
D = 14–16 cm when L = 120 cm; D = 12–15 cm when L = 360 cm [62]	CFD	Natural	Roof pitches	2009
22 cm [64]	CFD	Natural	Facades	2016
D = 23 cm when L = 400 cm [59]	CFD	Natural	Roof pitches	1997
D = 10 when L = 160 cm [61]	Experimental	Natural	Facades	2008
D/L = 0.05 [63,65]	Experimental and theoretical	Natural	Roof pitches	2006
D = 5–10 cm when L = 100 cm [66]	Experimental and theoretical	Natural	Roof pitches	2008
D/L = 0.11 [60]	Onsite tests	Forced	Roof pitches	2014

It can be noticed in Table 2 that the suggested gap depth based on the CFD results ranges from 12 to 23 cm for facades or roof pitches with natural ventilation, while the effects of gap length were not addressed in detail. Results from theoretical analysis [63,65] and an onsite experiment [60] showed that the temperature mitigation effects of the gap depth (D) are in collaboration with its length (L), and a shorter gap length is favorable for temperature mitigation. It was reported that the suggested D/L ratio ranged from 0.05 to 0.10. A strategy to reduce the gap length is to arrange the panels discontinuously as shown in Figure 3a.

In terms of forced ventilation, according to an experimental investigation [60], the power output was increased by 19% when forced ventilation was applied, after deducting the electricity used to power the fans. Therefore, use of additional fans for forced ventilation may be effective in terms of energy production, but it requires higher investments and maintenance and may cause noise. The forced ventilation may also be optimized to enable the fan operation to adjust according to the air temperature in the gap [67].

The heat from ventilation of BIPV facades is further utilized in some studies by incorporation with the Trombe wall system [30,68–70]. The mechanism is shown in Figure 4 where the heated air flow from the gap can be discharged to outside in summer and to interior side in winter. This helps to reduce the energy required for indoor heating in winter. In such applications, forced ventilation with a fan is usually used to accelerate the air flow [30]. The existing research and main results concerning the Trombe wall system comprising PV cells are listed in Table 3, and the main research approach is the combination of experiments and theoretical analysis or CFD simulation. It can be noticed in Table 3 that polycrystalline silicon (poly-Si) PV and a-Si PV cells were used in these studies, and the maximum temperatures in the PV cells were well controlled within 50 °C. However, this research only investigated the winter performance of the system, while the summer performance, where the PV performance would be more negatively affected, was not investigated. This is possibly because Trombe walls mainly function in winter, and the heat efficiency (usually over 20% according to Table 3) is much higher than the electrical efficiency of the PV cells. Future research is, therefore, required in terms of the possible performance degradation due to the elevated temperature in summer, in order to accurately predict the annual electrical and thermal performances of such applications.

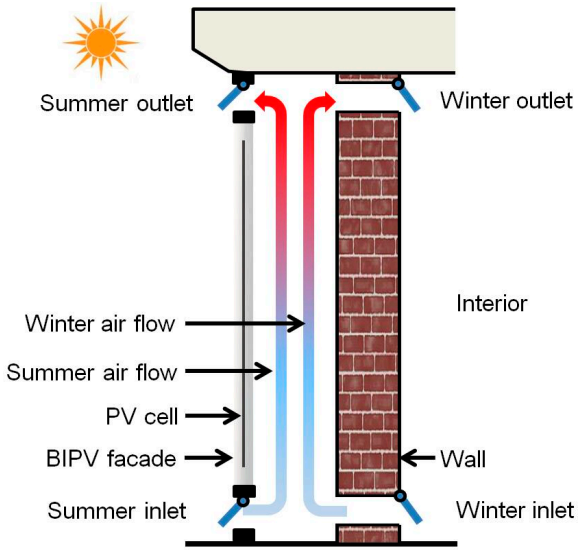

Figure 4. Mechanism of Trombe wall system with BIPV facade.

3.2. Water Circulation

When the PV cells were integrated with structural materials and ventilation from back side is largely prevented, the temperature elevation would be more obvious if no other approaches were applied [61]. A practical way is to introduce water circulation by embedded pipes to take away the excessive heat from the PV cells. In some studies, such a water circulation system is connected to heating systems of the building for room heating or providing hot water [31], and they are referred to as building integrated photovoltaic/thermal (BIPVT) systems in literature [71]. A brief summary of the research on BIPV systems with water circulation is presented in Table 4, where it can be noticed that both roof and vertical applications (walls and facades) have been investigated. Usually poly-Si or mono-Si silicon PV cells were used. CdTe PV cells were experimentally compared with c-Si in [72] and were found to have a smaller actual efficiency. The heat efficiency from outdoor experiments listed in Table 4 was taken as the average of annual data, and it ranges from 30 to 39%, while the results from theoretical analysis or indoor experiments were obtained at one or several fixed sunlight intensities and they range from 45 to 57%. The higher efficiency from theoretical analysis or indoor experiments may be attributed to the limited sunlight intensities investigated or the phase change materials (PCMs) applied. PCMs show potential to further increase the total efficiency of BIPV system with water circulation, but the effectiveness still requires validation from outdoor experiments. The heat efficiency in these systems is three to four times of the electrical efficiency of the PV cells; therefore, the heat collected from the PV cells should be further utilized, and the total efficiency would be much higher than the electrical efficiency of PV cells.

A prototype BIPVT roofing system was built [31] where c-Si PV modules were embedded between a transparent protective surface layer and a conductive aluminum back layer (thermal conductivity of 238 W/mK). Water pipes were attached to the aluminum layer, and then an insulating polyethylene layer (thermal conductivity of 0.26 W/mK) was applied at the bottom to prevent heat conduction to the building structure. This prototype had a dimension of about 0.5 × 0.6 m and was subjected to artificial sunlight. At a solar intensity of 850 W/m^2, the PV temperature ranged from 49 to 51 °C at different locations; and when a water flow with a temperature of 20 °C and a flow rate of 33 mL/min was applied, the temperature was reduced and ranged from 32 to 39 °C, and the temperature reduction was, therefore, 14.5 °C on average. Similarly, at a solar intensity of 1100 W/m^2, the PV temperature was reduced from 53–57 °C to 32–39 °C with a water flow rate of 66 mL/min. The prototype was designed to be integrated into building skin and the circulation water was planned to be further used for room heating.

Table 3. Temperature and efficiency results from research on Trombe wall system with BIPV facade.

Reference	Year	Location	PV Type	Research Method	PV Efficiency (%)	Max PV Temperature *	Heat Efficiency (%)	Season
Jie et al. [73]	2007	China	Poly-Si	Theoretical	14.7 (Rated: 14.0)	18 °C (5 °C, 700 W/m^2)	-	Winter
Jie et al. [74]	2007	China	Poly-Si	Experimental and theoretical	10.4 (Rated: 14.0)	44 °C (700 W/m^2)	-	Winter
Sun et al. [75]	2011	China	Poly-Si	Experimental and CFD	12.0	-	21.0	Winter
Koyunbaba et al. [76]	2013	Turkey	A-Si	Experimental and CFD	4.5	47 °C (21 °C, 751 W/m^2)	27.2	Winter-spring
Sharma and Kumari [69]	2016	Algeria	A-Si	CFD	3.7–4.2	40 °C (460 W/m^2)	-	Winter
Ahmed et al. [77]	2019	Iraq	Poly-Si	Experimental and theoretical	6.3/9.3 (without/with a fan) (Rated: 15.0)	58 °C (without fan) 39 °C (with a fan)	30.0 (without fan) 35.5 (with a fan)	Winter-spring

* Environment temperatures and sunlight intensities are provided in brackets if available.

Table 4. Research on BIPV systems with water circulation.

Reference	Year	Location	Research Method	PV Type	PV Efficiency (%)	Heat Efficiency	Scenario	Comment
Zondag et al. [78]	2003	Netherland	Experimental and theoretical	Poly-Si	5.8–6.7 (Rated: 10.3)	35–39%	Roof	Nine configurations were investigated.
Chow et al. [79]	2009	China	Experimental and theoretical	Poly-Si	9.4 (Rated: 13.0)	38%	Wall	Cost payback time was 14 years.
Kim et al. [80]	2013	Korean	Experimental	Mono-Si	17.0	30%	Roof	Max PV cell temperature: 45 °C (at 900 W/m^2)
Yin et al. [31]	2013	USA	Experimental (indoor)	Mono-Si	14.5 at 850 W/m^2 11.4 at 1100 W/m^2	54% (1000 W/m^2) 44% (850 W/m^2)	Roof	Two intensities were applied. Phase change materials (PCMs) were used.
Ibrahim et al. [81]	2014	Malaysia	Theoretical	Poly-Si	10.4–11.3 (Rated: 13.0)	45–51%	Roof	Max PV cell temperature: 54 °C (at 900 W/m^2)
Pugsley et al. [82]	2020	UK	Experimental and theoretical	Mono-Si	(Rated: 11.4)	-	Facade	Max PV cell temperature: 89 °C (at 870 W/m^2)
Xu et al. [72]	2020	China	Experimental and theoretical	C-Si/CdTe	C-Si: 11.2; CdTe: 8.3	>38%	Wall	Performance in three cities was compared.
Yao et al. [83]	2020	China	Theoretical	-	9.2 (Rated: 17.8)	57%	-	PCMs were used.

When the water circulation system in BIPVT applications is connected to a tank of water boiler and used as a pre-heating procedure, a control mechanism is required to balance the heat provided by the PV panels and the boiler for proper utilization of the heat from PV panels and supply enough hot water. For example, a BIPVT system was built in Korea [80], where c-Si PV modules were integrated into the roof and the water circulation was connected to a 500 L water tank of a boiler. In this application, the circulation would be switched on when the BIPVT temperature was over 4 °C higher than the water tank. A BIPV facade with a-Si PV cells was proposed for modelling in a recent study in 2019 [67], where the facade had a total area of 296.6 m^2 and its water circulation system was connected to a 3000 L water tank to assist the natural gas boiler. According to this estimation [67], the water-circulation system in the BIPV facade required an extra construction cost of EUR 29,160 and annual energy saving equivalent to EUR 4542, where the electricity cost was EUR 0.09/kWh; therefore, the cost payback time was about 7 years.

3.3. Phase Change Materials

Phase change materials (PCMs) absorb heat when transforming from solid phase to liquid, and emit heat in the solidification process [84]. In a recent study [85], a test room with a dimension of 3.0 × 2.4 × 3.1 m was fabricated with a BIPV facade comprising six CIGS PV cells. The PCM (paraffin wax, Rubitherm PCM RT 27) with a thickness of 40 mm was sealed in aluminum containers and mounted at the back side of the PV cells. The PCM material had a specific heat of 2000 J/kgK, latent heat of 189 kJ/kg, thermal conductivity of 0.2 W/mK, solidus temperature of 24.5 °C and liquidus temperature of 26.5 °C. The test configuration was then subjected to outdoor sunlight, where the maximum solar intensity was about 800 W/m^2. According to the results, the maximum operating temperatures of the PV cells were mitigated by 6–15 °C after the PCM were used. However the solidification could not be completed at night if the maximum daytime temperature was over 30 °C and solar intensity was over 800 W/m^2 [85]. Therefore, the PCM implementation needs to be designed with consideration of the local climate and building information. Additionally, in this research [85], an air gap of 120 mm was set at the backside of the PCMs for natural ventilation, suggesting that in single BIPV applications, two or more measures may be applied together to maintain the operating temperature of the integrated PV cells in a favorable range. For example, in another study [31], a prototype BIPV roof was fabricated with forced ventilation, PCMs and water circulation.

Due to the relatively low thermal conductivity (e.g., 0.2 W/mK for the paraffin wax in [85]) of PCMs, metal fins [86] or shreds [87] were added in the PCMs in some studies to improve the overall thermal conductivity and, therefore, temperature mitigation effects.

More research on BIPV systems with PCMs are presented in Table 5, and poly-Si, mono-Si and CIGS PV cells have been investigated in these studies. A wide range types of PCMs have been used, and PCMs in these studies were usually used for temperature mitigation of the integrated PV cells only, where the heat was not collected for further utilization. It should be noted that the rise of annual electrical power output is smaller than 6% (see Table 5). Considering that the heat efficiency may be over 30% for water circulation systems (see Table 4) and over 20% for Trombe wall systems (see Table 3), the heat collected by PCMs may also be further utilized, and it requires future research.

Table 5. Research on BIPV systems with PCM.

Reference	Year	Location	PV Type	Rise of Power Output	Research Method	Season	Scenario	PCM
Hasan et al. [88,89]	2010	Ireland	Poly-Si	-	Experimental	Indoor	Roof	Calcium chloride hexahydrate
Aelenei et al. [85,89]	2014	Portugal	Poly-Si	-	Experimental and theoretical	Winter	Facade	Gypsum board
Park et al. [90,91]	2014	South Korean	Poly-Si	1.0–1.5% (annual)	Experimental and theoretical	Annual	Facade	Paraffinic hydrocarbon
Hasan et al. [92]	2015	Ireland Pakistan	Poly-Si	6.2% (Ireland) 14.3% (Pakistan)	Experimental	Autumn	Roof	Capric–palmitic acid Calcium chloride hexahydrate
Maturi et al. [93]	2015	Italy	CIGS	2.3%	Experimental and FEM	Annual	Facade	-
Hasan et al. [94]	2017	United Arab Emirates	Poly-Si	6.0%	Experimental	Annual	Roof	PCM RT42
Alim et al. [91]	2020	Australia	Mono-Si	4.1% (winter) 2.2–4.3% (summer)	Experimental	Winter and summer	Roof tile	Methyl stearate
Curpek et al. [85]	2020	Czech Republic	CIGS	-	Experimental	Summer	Facade	Rubitherm PCM RT 27

4. Effects of Mechanical Loading on PV Cells

Mechanical loading introduces stresses and strains, and they may also affect the power output of BIPV applications. The effects of mechanical loading are well considered for the efficiency of the integrated PV cells [29] since existing BIPV components are mainly applied in the scenarios without structural loads. BIPV applications are, therefore, excluded from walls and other major load-carrying positions, which cover the major exterior surfaces of building where the majority of solar irradiation are received. Developing BIPV applications into walls and other load-carrying scenarios may expand the collection of solar energy for buildings. This requires understanding of electrical responses of different types of PV cells subjected to mechanical stresses or strains. A summary of mechanical experiments conducted on PV cells is presented in Table 6, where the critical strains for obvious degradation in electrical performance of the PV cells are also provided. In this case, mainly a-Si PV cells were investigated in existing studies due to their better resistance to mechanical strains.

Table 6. Mechanical experiments on PV cells.

Reference	Year	PV Type	Test Method	Cell Dimension	Critical Tensile Strain	Critical Compressive Strain
Jones et al. [95]	2003	A-Si	Bending	100 mm^2	0.75%	>1.70%
Sugar et al. [96]	2007	A-Si	Tension	98 × 36 mm^2	1.4%	
Kim et al. [97]	2011	Mono-Si	Tension	86 × 25 mm^2	0.3%	
Scotta et al. [98]	2016	A-Si	Tension	1700 × 1000 mm^2	1.5%	
Chen et al. [32]	2018	A-Si	Tension and compression	64 × 13 mm^2		0.50%
		Perovskite	Tension	100 × 13 mm^2	>3.0%	
Dai et al. [33]	2019	A-Si	Tension	270 × 45 mm^2	1.6%	
		Organic	Tension	20 mm wide	1.4%	
Dai et al. [99]	2019	A-Si	Compression	180 × 60 mm^2		<0.5%

4.1. Strain Effects on c-Si PV Cells and Their Structural Integrations

Several procedures and requirements are introduced in existing standards for mechanical loads on conventional PV panels such as c-Si PV cells [100]. For example, in order to sustain the loads caused by weather conditions, PV panels are required to operate normally at a static load of 2400 Pa or cyclic load of 1440 Pa for 10,000 cycles, applied uniformly on the front or back surface of the panels [101]. It should be noted that such loads are considerations of weather conditions only; therefore, effects of mechanical strains from structural loads are not addressed.

Experimental investigations were reported in literature to understand the effects of mechanical strains on electrical performance of c-Si PV cells. For example, three-point bending tests were conducted on c-Si PV cells, and the specimens indicated failure at a strain of 0.2% [102]. When c-Si PV cells were adhesively bonded by resin film or EVA (ethylene-vinyl acetate copolymer) film to carbon fiber reinforced polymer (CFRP) plates and subjected to 0.3% tensile load, obvious changes in the open-circuit voltage and short-circuit current were observed [97]. Commercial c-Si PV cells with 16.9% efficiency, a dimension of 74 × 32 mm and a thickness of 0.13 mm, were submitted to direct tensile loading and three-point bending in [103]. The results showed that the strength at breakage of the cells was 221 MPa at tension and 420 MPa at bending, while the corresponding strain was not specified [103]. A theoretical analysis was conducted in [104] to quantify the dependence of electrical current of c-Si PV cells on the tensile strain, and tensile experiments were also conducted to validate the theoretical results. At a tensile strain of

0.068%, the current reduction was only 3% according to theoretical results and 6% in the experiments [104]. Further research on theoretical prediction of strain-induced degradation in electrical performance of PV cells may be useful. For structural applications, c-Si PV cells were adhesively bonded to a curved sandwich structure on the surfaces of carbon fiber reinforced polymer (CFRP) with light-weight (29 kg/m^3) honeycomb core to manufacture wing profiles of airplanes. The curvature of the profile was 2 m^{-1}, and the integrated PV cells operated well under such a curvature [103].

4.2. Strain Effects on Thin-Film Flexible PV Cells and Their Structural Integrations

Although c-Si PV technology appears dominant in terms of market share, several types of thin-film flexible PV cells were also investigated with satisfactory performance under certain mechanical strain [33], showing potentials for load-carrying BIPV integrations. In this research, the critical tensile or compressive stain was determined when obvious degradation in open-circuit voltage, short-circuit current or power output was detected in the PV cells.

In an early work [95], a-Si PV cells were bent to fit cylinders of different radiuses to investigate the effects of mechanical strains on electrical performance of the a-Si PV cells. It was concluded that electrical performance of the cells began to degrade from a curvature of 1.2 cm^{-1} in tension, corresponding to a tensile strain of 0.75% in the a-Si layer, while the cell can be bent to 2.6 cm^{-1} curvature (corresponding to 1.7% compressive strain) without a noticeable change in electrical status as also shown in Table 6 [95]. Direct tensile tests were conducted on a-Si PV cells with a dimension of 270 × 45 mm^2, and no obvious changes in their open-circuit voltage and short-circuit current were observed prior to a tensile strain of 1.6% as shown in Table 6; after that, the degradation in electrical performance was attributed to cracking in the a-Si layer [33]. Tensile tests were conducted on a-Si PV cell specimens with a larger dimension (1700 × 1000 mm^2) and the critical tensile strain when an obvious reduction in the power output was reported as 1.5% in [98]. According to similar tensile experiments on a-Si PV cells in other research, the critical strain was determined to be about 1.4 [96] and 1.0% [32,105]. Therefore, the critical tensile strain for a-Si PV cells ranges from 0.8 to 1.6%, suggesting their feasibility in load-carrying scenarios for buildings.

In order to understand the effects of in-plane compressive strain on a-Si PV cells, the cells were adhesively bonded by an epoxy adhesive to GFRP square hollow sections and subjected to compressive loads [99]. GFRP materials were used due to their superior mechanical properties [106,107] and electrical insulation. The critical compressive strain was found to be related to the adhesive thickness, as it was about 0.2% for 2.0 mm adhesive and 0.5% for 0.5 mm adhesive, as also shown in Table 6. Similar experiments were conducted in [32] where the a-Si PV cells were bonded by polyimide tapes and the critical strain was 0.5%. Therefore, the critical strains for a-Si PV cells in compression were much smaller than those in tension. The effects of the adhesive layer were also noticed and investigated, where theoretical and numerical analyses were conducted to understand the strain transfer behavior through the adhesive layer [99]. It was found that strain transfer behavior was mainly affected by shear modulus and thickness of the adhesive layer as well as the elastic modulus, thickness and length of the PV cell. An approach to mitigate the mechanical strain transferred from the structural components to the integrated PV cells through adhesives with a low modulus (e.g., silicone adhesive) was, therefore, proposed, and the effectiveness was experimentally demonstrated [99]. In terms of structural applications, a-Si PV cells were integrated in the surfaces of solar-powered unmanned aerial vehicles. The a-Si PV cells had a thickness of 0.12 mm and could be bent with a radius of only 5 mm without noticeable degradation in their electrical characteristics [108].

Mechanical experiments have also been conducted on organic PV cells for BIPV applications. For example, organic PV cells on plastic foils with a total thickness of 0.2 mm were reported to operate normally when bent to a curvature of 5 mm^{-1} [109]. Tensile loads were directly applied on thin-film flexible organic PV cells, and the critical tensile strain

was determined to be 1.4% [33]. A review was conducted on the mechanical performance of organic PV cells in [55]. It was found that the decrease in electrical properties under tension or bending was attributed to the resistance change due to cracking of electrodes and active layers. In addition, it was suggested that a simple report of the bending radius was insufficient for describing the flexibility of organic PV cells, and since the PV cells are associated with a multi-layer structure, more details (such as thickness and mechanical properties of each layer) were necessary to calculate the strains on different layers of the PV cells in bending. Therefore, for PV cells to be applied in scenarios in association with tensile strains, direct application of tensile loads to induce continuous development of tensile strain is more reliable than application of a specified curvature [55].

5. Solar Irradiation Enhancement

5.1. Optimization of Location, Azimuth and Tilt

The annual solar energy cast to a project site can be estimated by established methods such as empirical formulas and previous records [37,110]. The sunlight intensity and its variation with time at the project site is the fundamental information to predict the power output of a PV project and determine the proper azimuth and tilt of the PV cells [111]. According to an evaluation on cost payback time of a proposed BIPV system comprising facade and roof applications based on the climate conditions of six cities in Brazil, the cost payback time would be 9 years in Rio de Janeiro but 23 years in Sao Paulo [51].

In order to understand the effects of azimuth and tilt on the power output of the PV cells in BIPV applications, an investigation of power output of PV panels with different azimuths and tilts was conducted based on the climate of Hong Kong and electrical properties of a typical c-Si PV module (SIEMENS SQ 175-PC) [27]. According to this result [27], for vertical specimens, south-facing ones produced the maximum electricity, while the output reduction was 29.4% for east-facing ones and 33.8% for the west-facing ones. For south-facing PV cells, the optimal tilt was 30°, and the output was reduced by 24.3% if the cells were horizontally placed or by 46.8% for vertical ones [27]. It can be seen that a vertical position is unfavorable for energy production; therefore, efforts have been made to place PV cells at an inclined position even in BIPV facades as shown in Figure 5.

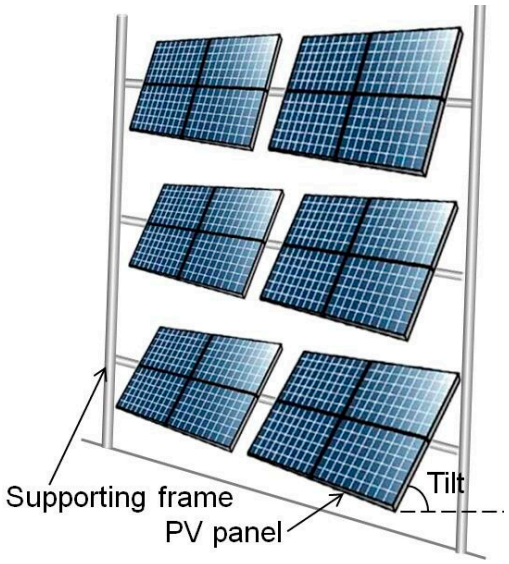

Figure 5. Integrated PV cells with a different tilt or azimuth to the facade.

The PV cells in Figure 5 may achieve an optimal tilt in facades by static supporting frame to produce the maximum electricity. The output could be further increased if the tile and azimuth could be changed with the position of the sun. In order to maximize the received solar irradiation, a dynamic BIPV facade was fabricated and installed in ETH

Zurich, Switzerland [36]. The facade covered a total area of 10 m^2 and had a total weight of 95 kg, comprising 30 modules capable of altering orientations in two axes. This BIPV facade system was able to detect the solar intensities at different directions and then alter the azimuth and tilt of the modules to receive the maximum solar intensity throughout the daytime. According to the results reported in [36], the dynamic BIPV facade was able to increase electricity gains by at least 50% compared to static ones. Similar dynamic PV systems were fabricated with a-Si PV cells and c-Si PV cells, respectively, in [112], and it was interesting that a-Si PV cells presented higher actual efficiency. According to a study reported in [113], the cost for fixed-tilt PV structures was USD 0.07 per watt output power, USD 0.12 per watt for the adjustable PV structures in one axis and USD 0.40 per watt for the two-axes ones [113].

The solar irradiation received by the integrated PV cells is also affected by shading, while the effect of shading is difficult to be estimated if the BIPV system is considered individually [51] since the PV cells may be shaded by surrounding buildings, trees and other facilities. A method was proposed to evaluate the BIPV performance at the urban scale, where models for all buildings and BIPV applications in the scale were established and the shading effect among buildings could be considered [112].

5.2. Transmittance of Surface Glazing

In order to avoid contamination, breakage and other damages to PV cells, the cells were encapsulated between a protective surface layer and a substrate in practice. The protective surface layer is highly transparent, usually with a transmittance of 90 to 96% [114]. However, the transmittance would decrease with dust accumulation in use. For example, the transmittance was found to decrease from 90.7 to 87.6% after use of 33 days [115], and the overall power output decreased by 50% after use of six months without cleaning [116]. A surface layer with high transmittance should, therefore, be chosen and cleaned regularly for higher power output of BIPV systems.

Self-clean coatings also help to mitigate dust accumulation and enhance dust removal at rain events [117]. A wide range of research has been conducted to develop effective self-clean coatings with low cost, high hydrothermal stability and high transparency. The major self-clean coatings are metal oxides such as silica, zinc oxide and alumina [115,117]. For example, an aluminum oxide self-cleaning coating with a thickness of 300 nm was developed on glass substrate without obvious compromise of its transmittance [117]. Contaminated PV panels with or without the coating were cleaned by water in the same way, while efficiency of the panels without the coating was recovered by 61% and that with the coating was recovered by 91%. This result suggests the effectiveness of the coating to maintain a better transmittance of the protective glass layer of the PV panels in use.

6. Conclusions

A review was conducted in this study with a focus on approaches to improve the power output of building integrated photovoltaic (BIPV) systems. These approaches are mainly associated with proper selection of the types of PV cells, the reduction in operational temperature and the enhancement for receiving solar irradiation.

In terms of different types of PV cells, crystalline silicon (c-Si) PV cells are reported with the highest efficiency and dominant market share, but their integrations with building materials must consider their brittleness and relatively thick configurations. Such c-Si PV cells are usually mounted by frames on rooftops or as facades in current BIPV applications. Amorphous silicon (a-Si) PV cells show potentials with their properties of thin film and flexibility. CdTe PV cells have superior energy payback time with thin-film or semi-transparent cells available in market, but their potential toxicity needs to be well addressed for applications in residential buildings. This concern is also raised for CIGS PV cells. BIPV applications with other PV cells, however, are still very limited, which may be opportunities for future research.

Approaches to mitigate the operating temperature of PV cells in BIPV applications were evaluated by considering both electrical efficiency and heat efficiency. Natural ventilation with an air gap is practical and widely applied, where a maximum reduction of 20 °C was reported. The gap depth was suggested to be the key parameter affecting the temperature mitigation and a proper depth was suggested as 12 to 23 cm or 5–10% of its total length. The heat collected by the gap may be further utilized by using the Trombe wall system, and the annual heat efficiency may be over 20%. Water circulation may also be applied, and further utilization of the heat may lead to a heat efficiency of over 30%. Considering the relatively higher heat efficiency than the electrical efficiency in these applications, the heat collected from PV cells is suggested to be utilized. Phase change materials are also applicable, but approaches to utilize the heat in PCMs require further research.

The mechanical effects on electrical performance of different PV cells have been investigated. However, the critical strain is about 0.2 to 0.3% for c-Si PV cells in tension or bending, 0.8 to 1.6% for a-Si PV cells in tension and 0.3 to 0.5% for a-Si PV cells in compression. Applicable load-carrying scenarios for these PV cells were, therefore, understood. Adhesive layers with low modulus were suggested to mitigate the mechanical strain transferred from structural components to the integrated PV cells. Several BIPV integration prototypes for load-carrying scenarios have been made, but future research is required to investigate their thermal and mechanical performance in outdoor environments.

Proper location, azimuth and tilt may obviously increase the solar energy received by the PV cells and therefore power output of BIPV systems. In some conventional BIPV applications, the location, azimuth and tilt were usually determined by the buildings. Efforts have been made for optimization with adjustable modules and other configurations. In order to reduce shading on the PV cells, the geometries of surrounding buildings and facilities should also be considered. Self-clean coatings were suggested in the protective surface layer of the PV cells to enhance the transmittance, and their effectiveness was experimentally verified, while cost effectiveness of adjustable modules and self-clean coatings still needs future investigations.

Author Contributions: Conceptualization, Y.B. and Y.D.; Methodology, Y.D.; Formal Analysis, Y.D.; Investigation, Y.D.; Writing—Original Draft Preparation, Y.D.; Writing—Review and Editing, Y.B.; Supervision, Y.B.; Project Administration, Y.B.; Funding Acquisition, Y.B. All authors have read and agreed to the published version of the manuscript.

Funding: The support from the Australian Research Council through the Discovery project (DP180102 208) is acknowledged.

Informed Consent Statement: Not applicable.

Data Availability Statement: The data presented in this study are available in the article.

Conflicts of Interest: The authors declare no conflict of interest. The funders had no role in the design of the study; in the collection, analyses, or interpretation of data; in the writing of the manuscript, or in the decision to publish the results.

Nomenclature

a-Si	Amorphous silicon
A(*t*)	Projected area of PV cell to sunlight at time t
BIPV	Building integrated Photovoltaic
BIPVT	Building integrated Photovoltaic thermal collectors
CIGS	Copper indium gallium selenide
CdTe	Cadmium telluride
CFD	Computational fluid dynamics
c-Si	Crystalline silicon
D	Depth of gap between PV cell and building envelope
E(*t*)	Actual efficiency of the PV cell at time t
EVA	Ethylene-vinyl acetate copolymer
FEM	Finite element method
FiT	Feed-in Tariff
GFRP	Glass fibre reinforced polymer
I(*t*)	Solar intensity at time t
L	Length of gap between PV cell and building envelope
Mono-Si	Monocrystalline silicon
PCM	Phase change material
Poly-Si	Polycrystalline silicon
P(*t*)	Electricity generated by PV cells
PV	Photovoltaic
Si	Silicon
t	Time
ΔT	Temperature difference between PV cells and environment

References

1. Hotopp, R. *Technical Requirements and Consultation Concept for Small Grid-Connected PV Plants within the German "1000-Roof PV Programme"*; Springer: Dordrecht, the Netherlands, 1991.
2. Sijm, J.P.M. *The Performance of Feed-In Tariffs to Promote Renewable Electricity in European Countries*; Energy Research Centre of the Netherlands ECN: Petten, The Netherlnds, 2002; Volume 7.
3. Rickerson, W.H.; Sawin, J.L.; Grace, R.C. If the Shoe FITs: Using Feed-In Tariffs to Meet U.S. Renewable Electricity Targets. *Electr. J.* **2007**, *20*, 73–86. [CrossRef]
4. Zhang, M.M.; Zhou, D.Q.; Zhou, P.; Liu, G.Q. Optimal feed-in tariff for solar photovoltaic power generation in China: A real options analysis. *Energy Policy* **2016**, *97*, 181–192. [CrossRef]
5. Martin, N.; Rice, J. The solar photovoltaic feed-in tariff scheme in New South Wales, Australia. *Energy Policy* **2013**, *61*, 697–706. [CrossRef]
6. Dinwoodie, T.L.; Shugar, D.S. Optimizing roof-integrated photovoltaics: A case study of the PowerGuard roofing tile. In Proceedings of the 1994 IEEE First World Conference on Photovoltaic Energy Conversion, Waikoloa, HI, USA, 5–9 December 1994.
7. Liu, B.; Duan, S.; Cai, T. Photovoltaic DC-Building-Module-Based BIPV System—Concept and Design Considerations. *IEEE Trans. Power Electron.* **2011**, *26*, 1418–1429. [CrossRef]
8. Peng, C.; Huang, Y.; Wu, Z. Building-Integrated Photovoltaics (BIPV) in Architectural Design in China. *Energy Build.* **2011**, *43*, 3592–3598. [CrossRef]
9. Hagemann, I. Architectural considerations for building-integrated photovoltaics. *Prog. Photovolt. Res. Appl.* **1996**, *4*, 247–258. [CrossRef]
10. Shukla, A.K.; Sudhakar, K.; Baredar, P. Recent advancement in BIPV product technologies: A review. *Energy Build.* **2017**, *140*, 188–195. [CrossRef]
11. Zdyb, A.; Żelazna, A.; Krawczak, E. Photovoltaic System Integrated Into the Noise Barrier—Energy Performance and Life Cycle Assessment. *J. Ecol. Eng.* **2019**, *20*, 183–188. [CrossRef]
12. Żelazna, A.; Gołębiowska, J.; Zdyb, A.; Pawłowski, A. A Hybrid vs. On-Grid Photovoltaic System: Multicriteria Analysis of Environmental, Economic, and Technical Aspects in Life Cycle Perspective. *Energies* **2020**, *13*, 3978. [CrossRef]
13. Kotarela, F.; Kyritsis, A.; Papanikolaou, N. On the Implementation of the Nearly Zero Energy Building Concept for Jointly Acting Renewables Self-Consumers in Mediterranean Climate Conditions. *Energies* **2020**, *13*, 1032. [CrossRef]
14. Torcellini, P.; Pless, S.; Deru, M.; Crawley, D.B. Zero Energy Buildings: A Critical Look at the Definition. In Proceedings of the 2006 ACEEE Summer Study on Energy Efficiency in Buildings, Pacific Grove, CA, USA, 14–18 August 2006.
15. Kerdan, I.G.; Raslan, R.; Ruyssevelt, P.; Gálvez, D.M. An exergoeconomic-based parametric study to examine the effects of active and passive energy retrofit strategies for buildings. *Energy Build.* **2016**, *133*, 155–171. [CrossRef]

16. Ming, H.; Qiu, Y. A comparison of building energy codes and policies in the USA, Germany, and China: Progress toward the net-zero building goal in three countries. *Clean Technol. Environ. Policy* **2019**, *21*, 291–305.
17. Lan, H.; Cheng, B.; Gou, Z.; Yu, R. An evaluation of feed-in tariffs for promoting household solar energy adoption in Southeast Queensland, Australia. *Sustain. Cities Soc.* **2020**, *53*, 101942. [CrossRef]
18. Ye, L.-C.; Rodrigues, J.F.D.; Lin, H.X. Analysis of feed-in tariff policies for solar photovoltaic in China 2011–2016. *Appl. Energy* **2017**, *203*, 496–505. [CrossRef]
19. Hoppmann, J.; Huenteler, J.; Girod, B. Compulsive policy-making—The evolution of the German feed-in tariff system for solar photovoltaic power. *Res. Policy* **2014**, *43*, 1422–1441. [CrossRef]
20. Ballif, C.; Perret-Aebi, L.-E.; Lufkin, S.; Rey, E. Integrated thinking for photovoltaics in buildings. *Nat. Energy* **2018**, *3*, 438–442. [CrossRef]
21. IEC. *Standard IEC 60904-3: Photovoltaic Devices. Part 3: Measurement Principles for Terrestrial Photovoltaic (PV) Solar Devices with Reference Spectral Irradiance Data*; IEC: Geneve, Switzerland, 2019.
22. ASTM. *ASTM-G173-03. Standard Tables for Reference Solar Spectral Irradiances: Direct Normal and Hemispherical on 37° Tilted Surface*; ASTM International: West Conshohocken, PA, USA, 2020.
23. Green, M.A.; Dunlop, E.D.; Hohl-Ebinger, J.; Yoshita, M.; Kopidakis, N.; Hao, X. Solar cell efficiency tables (version 56). *Prog. Photovolt. Res. Appl.* **2020**, *28*. [CrossRef]
24. Aaditya, G.; Pillai, R.; Mani, M. An insight into real-time performance assessment of a building integrated photovoltaic (BIPV) installation in Bangalore (India). *Energy Sustain. Dev.* **2013**, *17*, 431–437. [CrossRef]
25. Skoplaki, E.; Palyvos, J.A. On the temperature dependence of photovoltaic module electrical performance: A review of efficiency/power correlations. *Sol. Energy* **2009**, *83*, 614–624. [CrossRef]
26. Maturi, L.; Belluardo, G.; Moser, D.; Del Buono, M. BiPV System Performance and Efficiency Drops: Overview on PV Module Temperature Conditions of Different Module Types. *Energy Procedia* **2014**, *48*, 1311–1319. [CrossRef]
27. Lu, L.; Yang, H.X. Environmental payback time analysis of a roof-mounted building-integrated photovoltaic (BIPV) system in Hong Kong. *Appl. Energy* **2010**, *87*, 3625–3631. [CrossRef]
28. Lamnatou, C.; Notton, G.; Chemisana, D.; Cristofari, C. Storage systems for Building-Integrated Photovoltaic (BIPV) and Building-Integrated Photovoltaic/Thermal (BIPVT) installations: Environmental profile and other aspects. *Sci. Total Environ.* **2019**, *699*, 134269. [CrossRef] [PubMed]
29. Norton, B.; Eames, P.C.; Mallick, T.K.; Huang, M.J.; Mccormack, S.J.; Mondol, J.D.; Yohanis, Y.G. Enhancing the performance of building integrated photovoltaics. *Sol. Energy* **2011**, *85*, 1629–1664. [CrossRef]
30. Hu, Z.; He, W.; Ji, J.; Hu, D.; Lv, S.; Chen, H.; Shen, Z. Comparative study on the annual performance of three types of building integrated photovoltaic (BIPV) Trombe wall system. *Appl. Energy* **2017**, *194*, 81–93. [CrossRef]
31. Yin, H.M.; Yang, D.J.; Kelly, G.; Garant, J. Design and performance of a novel building integrated PV/thermal system for energy efficiency of buildings. *Sol. Energy* **2013**, *87*, 184–195. [CrossRef]
32. Chen, A.; Yossef, M.; Zhang, C. Strain effect on the performance of amorphous silicon and perovskite solar cells. *Sol. Energy* **2018**, *163*, 243–250. [CrossRef]
33. Dai, Y.; Huang, Y.; He, X.; Hui, D.; Bai, Y. Continuous performance assessment of thin-film flexible photovoltaic cells under mechanical loading for building integration. *Sol. Energy* **2019**, *183*, 96–104. [CrossRef]
34. Shang, C.; Wei, P. Enhanced support vector regression based forecast engine to predict solar power output. *Renew. Energy* **2018**, *127*, 269–283. [CrossRef]
35. Ma, Y.; Li, G.; Tang, R. Optical performance of vertical axis three azimuth angles tracked solar panels. *Appl. Energy* **2011**, *88*, 1784–1791. [CrossRef]
36. Svetozarevic, B.; Begle, M.; Jayathissa, P.; Caranovic, S.; Shepherd, R.; Nagy, Z.; Hofer, J.; Schlueter, A. Dynamic photovoltaic building envelopes for adaptive energy and comfort management. *Nat. Energy* **2019**, *4*, 671–682. [CrossRef]
37. Evans, D.L. Simplified method for predicting photovoltaic array output. *Sol. Energy* **1981**, *27*, 555–560. [CrossRef]
38. Jelle, B.P.; Breivik, C.; Røkenes, H.D. Building Integrated Photovoltaic Products: A State-of-the-Art Review and Future Research Opportunities. *Sol. Energy Mater. Sol. Cells* **2012**, *100*, 69–96. [CrossRef]
39. Tripathy, M.; Sadhu, P.K.; Panda, S.K. A critical review on building integrated photovoltaic products and their applications. *Renew. Sustain. Energy Rev.* **2016**, *61*, 451–465. [CrossRef]
40. Feldman, D.; Margolis, R. *Solar Industry Update Q4 2018/Q1 2019*; National Renewable Energy Laboratory (NREL): Golden, CO, USA, 2019.
41. Lee, T.D.; Ebong, A.U. A review of thin film solar cell technologies and challenges. *Renew. Sustain. Energy Rev.* **2017**, *70*, 1286–1297. [CrossRef]
42. Virtuani, A.; Pavanello, D.; Friesen, G. Overview of Temperature Coefficients of Different Thin Film Photovoltaic Technologies. In Proceedings of the 5th World Conference on Photovoltaic Energy Conversion, Valencia, Spain, 6–10 September 2010; pp. 4248–4252.
43. Jungbluth, N.; Dones, R.; Frischknecht, R. Life Cycle Assessment of Photovoltaics Update of the ecoinvent Database. *MRS Proc.* **2007**, *1041*, R01–R03. [CrossRef]
44. Pascual, C.; Castro, J.d.; Schueler, A.; Keller, T. Integration of dye solar cells in load-bearing translucent glass fiber-reinforced polymer laminates. *J. Compos. Mater.* **2016**, *51*. [CrossRef]

45. Roy, A.; Ghosh, A.; Bhandari, S.; Selvaraj, P.; Mallick, T.K. Colour Comfort Evaluation of Dye Sensitized Solar Cell (DSSC) Based Building Integrated Photovoltaic (BIPV) Glazing after Two Years of Ambient Exposure. *J. Phys. Chem. C* **2019**, *123*, 23834–23837. [CrossRef]
46. Gholami, H.; Røstvik, H.N.; Kumar, N.M.; Chopra, S.S. Lifecycle cost analysis (LCCA) of tailor-made building integrated photovoltaics (BIPV) façade: Solsmaragden case study in Norway. *Sol. Energy* **2020**, *211*, 488–502. [CrossRef]
47. Lin, Q.; Huang, H.; Jing, Y.; Fu, H.; Chang, P.; Li, D.; Yao, Y.; Fan, Z. Flexible photovoltaic technologies. *J. Mater. Chem. C* **2014**, *2*, 1233–1247. [CrossRef]
48. Aelenei, D.; Lopes, R.A.; Aelenei, L.; Goncalves, H. Investigating the potential for energy flexibility in an office building with a vertical BIPV and a PV roof system. *Renew. Energy* **2019**, *137*, 189–197. [CrossRef]
49. Shahrestani, M.; Yao, R.; Essah, E.; Shao, L.; Oliveira, A.C.; Hepbasli, A.; Biyik, E.; Caño, T.d.; Rico, E.; Lechón, J.L. Experimental and numerical studies to assess the energy performance of naturally ventilated PV facade systems. *Sol. Energy* **2017**, *147*, 37–51. [CrossRef]
50. Yang, J.; Banerjee, A.; Guha, S. Triple-junction amorphous silicon alloy solar cell with 14.6% initial and 13.0% stable conversion efficiencies. *Appl. Phys. Lett.* **1997**, *70*, 2975–2977. [CrossRef]
51. Sorgato, M.J.; Schneider, K.; Rüther, R. Technical and economic evaluation of thin-film CdTe building-integrated photovoltaics (BIPV) replacing façade and rooftop materials in office buildings in a warm and sunny climate. *Renew. Energy* **2018**, *118*, 84–98. [CrossRef]
52. Aliyu, M.M.; Islam, M.A.; Hamzah, N.R.; Karim, M.R.; Matin, M.A.; Sopian, K.; Amin, N. Recent Developments of Flexible CdTe Solar Cells on Metallic Substrates: Issues and Prospects. *Int. J. Photoenergy* **2012**, *2012*, 351381. [CrossRef]
53. Alrashidi, H.; Ghosh, A.; Issa, W.; Sellami, N.; Mallick, T.K.; Sundaram, S. Thermal performance of semitransparent CdTe BIPV window at temperate climate. *Sol. Energy* **2020**, *195*, 536–543. [CrossRef]
54. Major, J.D.; Treharne, R.E.; Phillips, L.J.; Durose, K. A low-cost non-toxic post-growth activation step for CdTe solar cells. *Nature* **2014**, *511*, 334–337. [CrossRef]
55. Savagatrup, S.; Printz, A.D.; O'Connor, T.F.; Zaretski, A.V.; Rodriquez, D.; Sawyer, E.J.; Rajan, K.M.; Acosta, R.I.; Root, S.E.; Lipomi, D.J. Mechanical degradation and stability of organic solar cells: Molecular and microstructural determinants. *Energy Environ. Sci.* **2014**, *8*, 55–80. [CrossRef]
56. Ng, C.H.; Lim, H.N.; Hayase, S.; Zainal, Z.; Huang, N.M. Photovoltaic performances of mono- and mixed-halide structures for perovskite solar cell: A review. *Renew. Sustain. Energy Rev.* **2018**, *90*, 248–274. [CrossRef]
57. Eke, R.; Senturk, A. Monitoring the performance of single and triple junction amorphous silicon modules in two building integrated photovoltaic (BIPV) installations. *Appl. Energy* **2013**, *109*, 154–162. [CrossRef]
58. Saadon, S.; Gaillard, L.; Giroux, S.; Ménézo, C. Simulation Study of a Naturally Ventilated Building Integrated Photovoltaic (BIPV) Envelope. *Energy Procedia* **2015**, *87*, 517–531. [CrossRef]
59. Brinkworth, B.J.; Cross, B.M.; Marshall, R.H.; Yang, H. Thermal regulation of photovoltaic cladding. *Sol. Energy* **1997**, *61*, 169–178. [CrossRef]
60. Kaiser, A.S.; Zamora, B.; Mazón, R.; García, J.R.; Vera, F. Experimental study of cooling BIPV modules by forced convection in the air channel. *Appl. Energy* **2014**, *135*, 88–97. [CrossRef]
61. Fossa, M.; Ménézo, C.; Leonardi, E. Experimental natural convection on vertical surfaces for building integrated photovoltaic (BIPV) applications. *Exp. Thermal Fluid Sci.* **2008**, *32*, 980–990. [CrossRef]
62. Gan, G. Effect of air gap on the performance of building-integrated photovoltaics. *Energy* **2009**, *34*, 913–921. [CrossRef]
63. Brinkworth, B.J.; Sandberg, M. Design procedure for cooling ducts to minimise efficiency loss due to temperature rise in PV arrays. *Sol. Energy* **2006**, *80*, 89–103. [CrossRef]
64. Elsayed, M.S. Optimizing thermal performance of building-integrated photovoltaics for upgrading informal urbanization. *Energy Build.* **2016**, *116*, 232–248. [CrossRef]
65. Brinkworth, B.J. Optimum depth for PV cooling ducts. *Sol. Energy* **2006**, *80*, 1131–1134. [CrossRef]
66. Tonui, J.K.; Tripanagnostopoulos, Y. Performance improvement of PV/T solar collectors with natural air flow operation. *Sol. Energy* **2008**, *82*, 1–12. [CrossRef]
67. Martin-Escudero, K.; Salazar-Herran, E.; Campos-Celador, A.; Diarce-Belloso, G.; Gomez-Arriaran, I. Solar Energy system for heating and domestic hot water supply by means of a heat pump coupled to a photovoltaic ventilated façade. *Sol. Energy* **2019**, *183*, 453–462. [CrossRef]
68. Irshad, K.; Habib, K.; Thirumalaiswamy, N. Performance Evaluation of PV-trombe Wall for Sustainable Building Development. *Procedia CIRP* **2015**, *26*, 624–629. [CrossRef]
69. Sharma, S.L.; Kumari, K. Numerical study of natural ventilation in BIPV trombe wall. *GRD J.* **2016**, *1*, 34–41.
70. Xu, X. Modeling of Natural Ventilation in Built-in Photovoltaic-Trombe Wall. *Appl. Mech. Mater.* **2013**, *448–453*, 1537–1541. [CrossRef]
71. Pereira, R.; Aelenei, L. Optimization assessment of the energy performance of a BIPV/T-PCM system using Genetic Algorithms. *Renew. Energy* **2019**, *137*, 157–166. [CrossRef]
72. Xu, L.; Ji, J.; Luo, K.; Li, Z.; Xu, R.; Huang, S. Annual analysis of a multi-functional BIPV/T solar wall system in typical cities of China. *Energy* **2020**, *197*, 117098. [CrossRef]

73. Jie, J.; Hua, Y.; Wei, H.; Gang, P.; Jianping, L.; Bin, J. Modeling of a novel Trombe wall with PV cells. *Build. Environ.* **2007**, *42*, 1544–1552. [CrossRef]
74. Jie, J.; Hua, Y.; Gang, P.; Jianping, L. Study of PV-Trombe wall installed in a fenestrated room with heat storage. *Appl. Thermal Eng.* **2007**, *27*, 1507–1515. [CrossRef]
75. Sun, W.; Ji, J.; Luo, C.; He, W. Performance of PV-Trombe wall in winter correlated with south façade design. *Appl. Energy* **2011**, *88*, 224–231. [CrossRef]
76. Koyunbaba, B.K.; Yilmaz, Z.; Ulgen, K. An approach for energy modeling of a building integrated photovoltaic (BIPV) Trombe wall system. *Energy Build.* **2013**, *67*, 680–688. [CrossRef]
77. Ahmed, O.K.; Hamada, K.I.; Salih, A.M. Enhancement of the performance of Photovoltaic/Trombe wall system using the porous medium: Experimental and theoretical study. *Energy* **2019**, *171*, 14–26. [CrossRef]
78. Zondag, H.A.; de Vries, D.W.; van Helden, W.G.J.; van Zolingen, R.J.C.; van Steenhoven, A.A. The yield of different combined PV-thermal collector designs. *Sol. Energy* **2003**, *74*, 253–269. [CrossRef]
79. Chow, T.T.; Chan, A.L.S.; Fong, K.F.; Lin, Z.; He, W.; Ji, J. Annual performance of building-integrated photovoltaic/water-heating system for warm climate application. *Appl. Energy* **2009**, *86*, 689–696. [CrossRef]
80. Kim, J.-H.; Park, S.-H.; Kang, J.-G.; Kim, J.-T. Experimental Performance of Heating System with Building-integrated PVT (BIPVT) Collector. *Energy Procedia* **2014**, *48*, 1374–1384. [CrossRef]
81. Ibrahim, A.; Fudholi, A.; Sopian, K.; Othman, M.Y.; Ruslan, M.H. Efficiencies and improvement potential of building integrated photovoltaic thermal (BIPVT) system. *Energy Convers. Manag.* **2014**, *77*, 527–534. [CrossRef]
82. Pugsley, A.; Zacharopoulos, A.; Mondol, J.D.; Smyth, M. BIPV/T facades—A new opportunity for integrated collector-storage solar water heaters? Part 2: Physical realisation and laboratory testing. *Sol. Energy* **2020**, *206*, 751–769. [CrossRef]
83. Yao, J.; Xu, H.; Dai, Y.; Huang, M. Performance analysis of solar assisted heat pump coupled with build-in PCM heat storage based on PV/T panel. *Sol. Energy* **2020**, *197*, 279–291. [CrossRef]
84. Marta, K.; Dominika, M.; Michał, W.T. The role of phase change materials for the sustainable energy. *E3S Web Conf.* **2016**, *10*. [CrossRef]
85. Cekon, J.C.M. Climate response of a BiPV faade system enhanced with latent PCM-based thermal energy storage. *Renew. Energy* **2020**, *152*, 368–384.
86. Huang, M.J. The effect of using two PCMs on the thermal regulation performance of BIPV systems. *Sol. Energy Mater. Sol. Cells* **2011**, *95*, 957–963. [CrossRef]
87. Maiti, S.; Banerjee, S.; Vyas, K.; Patel, P.; Ghosh, P.K. Self regulation of photovoltaic module temperature in V-trough using a metal–wax composite phase change matrix. *Sol. Energy* **2011**, *85*, 1805–1816. [CrossRef]
88. Hasan, A.; McCormack, S.J.; Huang, M.J.; Norton, B. Evaluation of phase change materials for thermal regulation enhancement of building integrated photovoltaics. *Sol. Energy* **2010**, *84*, 1601–1612. [CrossRef]
89. Aelenei, L.; Pereira, R.; Gonçalves, H.; Athienitis, A. Thermal Performance of a Hybrid BIPV-PCM: Modeling, Design and Experimental Investigation. *Energy Procedia* **2014**, *48*, 474–483. [CrossRef]
90. Park, J.; Kim, T.; Leigh, S.-B. Application of a phase-change material to improve the electrical performance of vertical-building-added photovoltaics considering the annual weather conditions. *Sol. Energy* **2014**, *105*, 561–574. [CrossRef]
91. Alim, M.A.; Tao, Z.; Abden, M.J.; Rahman, A.; Samali, B. Improving performance of solar roof tiles by incorporating phase change material. *Sol. Energy* **2020**, *207*, 1308–1320. [CrossRef]
92. Hasan, A.; McCormack, S.J.; Huang, M.J.; Sarwar, J.; Norton, B. Increased photovoltaic performance through temperature regulation by phase change materials: Materials comparison in different climates. *Sol. Energy* **2015**, *115*, 264–276. [CrossRef]
93. Maturi, L.; Lollini, R.; Moser, D.; Sparber, W. Experimental investigation of a low cost passive strategy to improve the performance of Building Integrated Photovoltaic systems. *Sol. Energy* **2015**, *111*, 288–296. [CrossRef]
94. Hasan, A.; Sarwar, J.; Alnoman, H.; Abdelbaqi, S. Yearly energy performance of a photovoltaic-phase change material (PV-PCM) system in hot climate. *Sol. Energy* **2017**, *146*, 417–429. [CrossRef]
95. Jones, R.; Johnson, T.; Jordan, W.; Wagner, S.; Guha, S. Effects of mechanical strain on the performance of amorphous silicon triple-junction solar cells. In Proceedings of the 29th IEEE Photovoltaic Specialists Conference, New Orleans, LA, USA, 19–24 May 2002.
96. Sugar, J.G.; Scaffaro, R.; Guo, Z.; Maung, J.K.; Hahn, H.T. Photovoltaic performance of amorphous silicon flexible solar modules under mechanical loading. In Proceedings of the 6th International Workshop on Structural Health Monitoring, Stanford, CA, USA, 11–13 September 2007.
97. Kim, J.; Choi, I.; Kim, D.; Cheong, S. Development of Single Crystalline Silicon Solar Cells Lay-Down Process on Composites. In Proceedings of the 18th International Conference on Composite Materials, Jeju Island, Korea, 21–26 August 2011.
98. Scotta, R.; Lazzari, M.; Stecca, E.; Di Massimo, R.; Vitaliani, R. Membranes with embedded photovoltaic flexible cells: Structural and electrical performances under uniaxial and biaxial stresses. *Compos. Struct.* **2016**, *157*, 111–120. [CrossRef]
99. Dai, Y.; Bai, Y.; Keller, T. Stress mitigation for adhesively bonded photovoltaics with fibre reinforced polymer composites in load carrying applications. *Compos. Part B Eng.* **2019**, *177*, 107420. [CrossRef]
100. IEC. *IEC-61215-1:2016. Terrestrial Photovoltaic (PV) Modules—Design Qualification and Type Approval—Part 1: Test Requirements*; IEC: Geneva, Swizerland, 2016.

101. ASTM. *ASTM-E1830-15. Standard Test Methods for Determining Mechanical Integrity of Photovoltaic Modules*; ASTM International: West Conshohocken, PA, USA, 2019.
102. Kang, J. *Structural Integration of Silicon Solar Cells and Lithium-Ion Batteries Using Printed Electronics*; Hahn, H.T., Carman, G., Chiou, P.-Y., Pei, Q., Eds.; ProQuest Dissertations Publishing: Los Angeles, CA, USA, 2012.
103. Rion, J.; Leterrier, Y.; Manson, J.-A.E.; Blairon, J.-M. Ultra-light asymmetric photovoltaic sandwich structures. *Composites Part A Appl. Sci. Manuf.* **2009**, *40*, 1167–1173. [CrossRef]
104. Guin, L.; Cabarrocas, P.R.I.; Jabbour, M.E.; Triantafyllidis, N. Effect of strain on the dark current-voltage characteristic of silicon heterojunction solar cells. *Sol. Energy* **2020**, *196*, 457–461. [CrossRef]
105. Yossef, M.; Chen, A. Strain Effect on the Performance of Solar Cells. In Proceedings of the 15th Biennial ASCE International Conference on Engineering, Science, Construction and Operations in Challenging Environments, Orlando, FL, USA, 11–15 April 2016.
106. Dai, Y.; Dai, X.; Bai, Y.; He, X. Aerodynamic Performance of an Adaptive GFRP Wind Barrier Structure for Railway Bridges. *Materials* **2020**, *13*, 4214. [CrossRef] [PubMed]
107. Gu, X.; Dai, Y.; Jiang, J. Flexural behavior investigation of steel-GFRP hybrid-reinforced concrete beams based on experimental and numerical methods. *Eng. Struct.* **2020**, *206*, 110117.
108. Kishi, Y.; Inoue, H.; Murata, K.; Tanaka, H.; Kouzuma, S.; Morizane, M.; Fukuda, Y.; Nishiwaki, H.; Nakano, K.; Takeoka, A.; et al. Ultralight flexible amorphous silicon solar cell and its application to an airplane. *Sol. Energy Mater.* **1991**, *23*, 312–318. [CrossRef]
109. Kaltenbrunner, M.; White, M.S.; Glowacki, E.D.; Sekitani, T.; Someya, T.; Sariciftci, N.S.; Bauer, S. Ultrathin and lightweight organic solar cells with high flexibility. *Nat. Commun.* **2012**, *3*, 770. [CrossRef] [PubMed]
110. Reikard, G. Predicting solar radiation at high resolutions: A comparison of time series forecasts. *Sol. Energy* **2009**, *83*, 342–349. [CrossRef]
111. Shukla, A.K.; Sudhakar, K.; Baredar, P. A comprehensive review on design of building integrated photovoltaic system. *Energy Build.* **2016**, *128*, 99–110. [CrossRef]
112. Kang, H.; Hong, T.; Jung, S.; Lee, M. Techno-economic performance analysis of the smart solar photovoltaic blinds considering the photovoltaic panel type and the solar tracking method. *Energy Build.* **2019**, *193*, 1–14. [CrossRef]
113. Rodríguez-Gallegos, C.D.; Liu, H.; Gandhi, O.; Singh, J.P.; Krishnamurthy, V.; Kumar, A.; Stein, J.S.; Wang, S.; Li, L.; Reindl, T.; et al. Global Techno-Economic Performance of Bifacial and Tracking Photovoltaic Systems. *Joule* **2020**, *4*, 1514–1541. [CrossRef]
114. Pascual, C.; de Castro, J.; Schueler, A.; Vassilopoulos, A.P.; Keller, T. Total light transmittance of glass fiber-reinforced polymer laminates for multifunctional load-bearing structures. *J. Compos. Mater.* **2014**, *48*, 3591–3604. [CrossRef]
115. Hee, J.Y.; Kumar, L.V.; Danner, A.J.; Yang, H.; Bhatia, C.S. The Effect of Dust on Transmission and Self-cleaning Property of Solar Panels. *Energy Procedia* **2012**, *15*, 421–427. [CrossRef]
116. Adinoyi, M.J.; Said, S.A.M. Effect of dust accumulation on the power outputs of solar photovoltaic modules. *Renew. Energy* **2013**, *60*, 633–636. [CrossRef]
117. Sutha, S.; Suresh, S.; Raj, B.; Ravi, K.R. Transparent alumina based superhydrophobic self–cleaning coatings for solar cell cover glass applications. *Sol. Energy Mater. Sol. Cells* **2017**, *165*, 128–137. [CrossRef]